Power Quality Assessment Using Signal Periodicity Independent Algorithms – A Shipboard Microgrid Case Study

Terriche, Yacine; Lashab, Abderezak; Çimen, Halil; Guerrero, Josep M.; Su, chun Lien; Vasquez, Juan C.

Published in:
Applied Energy

DOI (link to publication from Publisher):
10.1016/j.apenergy.2021.118151

Publication date:
2022

Document Version
Publisher's PDF, also known as Version of record

Applied Energy 307 (2022) 118151

Contents lists available at ScienceDirect

Applied Energy

journal homepage: www.elsevier.com/locate/apenergy

Power quality assessment using signal periodicity independent algorithms – A shipboard microgrid case study☆

Yacine Terriche [a,*], Abderezak Lashab [a], Halil Çimen [a], Josep M. Guerrero [a], Chun-Lien Su [b], Juan C. Vasquez [a]

[a] The Department of Energy Technology, Aalborg University, Aalborg 9220, Denmark
[b] The Department of Electrical Engineering, National Kaohsiung University of Science and Technology, Kaohsiung, Taiwan

HIGHLIGHTS

- Investigating and revealing potential risks of poor energy quality for shipboard microgrids.
- Providing a clear view of the importance of selecting the accurate algorithms for analyzing the quality of energy and delivering a comparative study.
- Proposing a developed algorithm, which is an offline-based energy quality analyzing technique developed for the short-term protective action stage to assess the energy quality of shipboard microgrids.
- Proposing an enhanced algorithm, which is an online-based energy quality assessing technique, Which is very suitable for the long-term preventive action stage.

ARTICLE INFO

Keywords:
Shipboard microgrids
Discrete Fourier Transform (DFT)
Energy quality assessment
Fast Fourier Transform (FFT)
Harmonic analysis
Eigenvalue solution
Singular value decomposition

ABSTRACT

Retrofitting of shipboard microgrids is receiving much attention nowadays due to the flexibility it offers to adapt existing ships with rapid market variations to move towards all-electric ships (A-ESs). This modernity mainly relies on incorporating the power electronics converters that unfortunately draw a large number of harmonics, which affect the energy quality and threaten the system stability and crew/passengers safety. The contribution of this paper lies in proposing two developed open-loop algorithms to assess the harmonics distortion of A-ESs without relying on signal periodicity. The first algorithm is an offline-based analyzing technique developed for the short-term protective action stage, which incorporates the eigenvalue solution inside the short-time fast Fourier transform (ST-FFT) to adapt its window size. Consequently, this algorithm can provide a comprehensive harmonics analysis with a fast transient response even under large system frequency drifts. The second algorithm is an online-based assessing technique, which is very suitable for the long-term preventive action stage to provide accurate harmonics distortion assessment with the fast transient response and efficient computation burden. This approach relies on cascading three moving average filters (MAFs) with particular window sizes to filter and estimate the mean value inside the discrete Fourier transform and the true RMS blocks without the need of frequency information. Hence, it results in enhancing the harmonics rejection capability of the algorithm even under the existence of non-characteristic harmonics and frequency drifts. Simulation and experimental results are provided to validate the efficacy of the proposed algorithms and the results are compared with traditional methods.

1. Introduction

Over recent years, the widespread utilization of power electronics converters (PECs) has caused considerable energy quality issues, particularly harmonic pollution in electrical power systems (EPSs). In particular, the tremendous evolution of retrofitted ships in moving

☆ This work was supported by VILLUM FONDEN under the VILLUM Investigator Grant (no. 25920): Center for Research on Microgrids (CROM). The work of Chun-Lien Su was funded by the Ministry of Science and Technology of Taiwan under Grant MOST 110-2221-E-992-044-MY3.

* Corresponding author.
E-mail addresses: yte@et.aau.dk (Y. Terriche), abl@et.aau.dk (A. Lashab), haci@energy.aau.dk (H. Çimen), joz@et.aau.dk (J.M. Guerrero), cls@nkust.edu.tw (C.-L. Su), juq@et.aau.dk (J.C. Vasquez).

https://doi.org/10.1016/j.apenergy.2021.118151
Received 17 August 2021; Received in revised form 10 October 2021; Accepted 29 October 2021
Available online 15 November 2021

towards all-electric ships (A-ESs) requires the applications of the PECs to provide enhanced maneuverability, controllability, and efficiency [1,2]. This advancement, however, results in affecting the energy quality of the EPS. The existence of harmonics onboard A-ESs not only affects their EPS efficiency but also threatens the lives of the ship crew/passengers, as well as increases some specific emissions [3–5].

Acquiring accurate information of the existing harmonics under different operating modes of A-ESs is crucial for engineers to assess the level of the total harmonic distortion (THD) and verify if the quality of energy complies with the norms. Precise analysis of the energy quality helps also to design suitable compensators, taking into consideration some important criteria such as the type of harmonics (odd/even harmonics, integer/non-integer multiple of the fundamental frequency), and the level of distortion [1]. Furthermore, energy quality analysis can provide a comprehension diagnosis for fault detection, and fault location of the synchronous generators and motors [6,7]. RMS Queen Marry II (QM II) transatlantic ocean liner is a high-profile example of the disastrous accident of harmonics [8], therefore, harmonics analysis onboard ships is very essential from the safety and efficiency point of view. Fig. 1 presents a generic EPS of an AC ship, which constitutes diesel generators, propulsion motors, thrusters, energy storage systems, hotel loads, and cold ironing. In most AC ships, the propulsion motors and thrusters consume about 80% to 90% of the total power. The integration of the voltage frequency drives (VFDs) to control these motors draws a large number of harmonics as shown in the experimental data of a bulk carrier ship in Fig. 1.

In order to elaborate the harmonics assessment process onboard shipboard power system, Fig. 2 is presented. The procedure is divided into two main stages. The first stage is a consulting action, which is taken by recording the data of the voltage/current sources, the main switchboard, and each outbreak busbar to provide a comprehensive harmonics assessment under different operation modes of the ship. If the harmonics distortion respects the norms, then it is not necessary to proceed to take any prevention action. However, if the harmonics distortion level exceeds the norms, taking the prevention long-term action becomes a mandatory task. The prevention action requires the installation of permanent measurement devices for each outbreak busbar connected to the main switchboard. Under certain operating modes, if the harmonics contamination becomes severe due to certain expected/unexpected reasons, particularly for the supplied voltage, the permanent measurement devices send information to the power management system to connect the filters if they are available or disconnect the affected busbar to avoid the disastrous consequences that can lead to the blackout of the ship. Hence, from the application point of view, the techniques of evaluating the harmonics for the consulting action might differ from those that are applied for the preventing action in terms of accuracy, computation burden, and the number of aiding parameters.

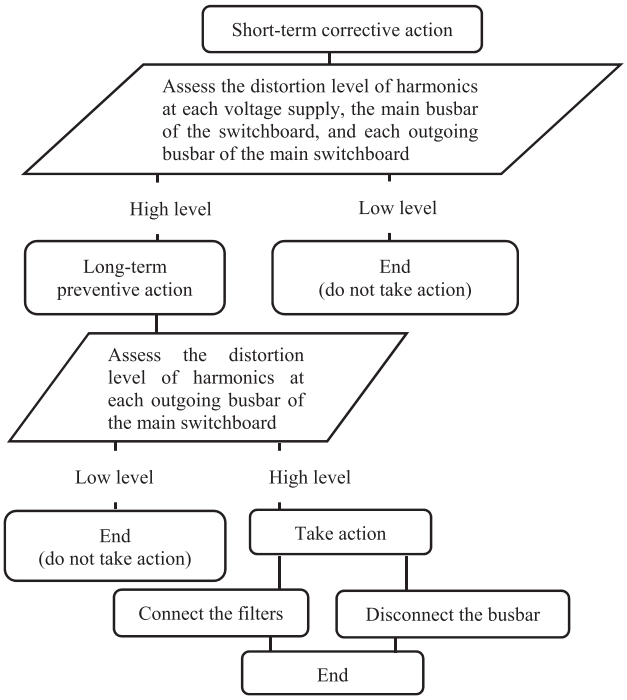

Fig. 2. A systematic approach to assess the harmonics and take corrective actions onboard A-ESs.

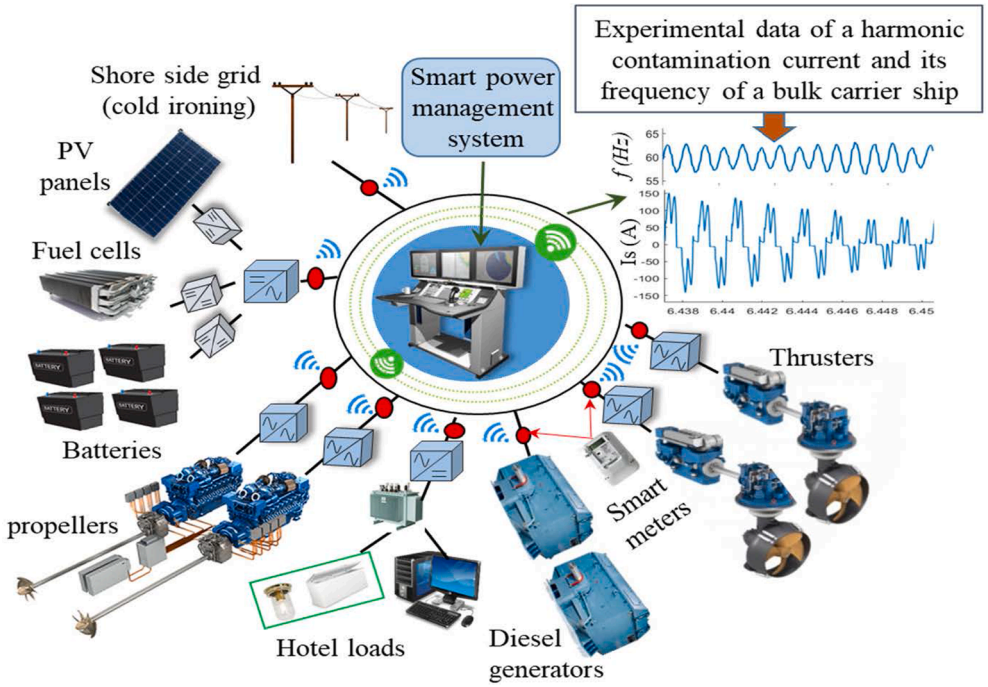

Fig. 1. A generic scheme of a smart AC shipboard microgrids.

For example, the long-term preventive action stage (L-TPAS) requires online techniques that prioritize low computation methods and some aiding parameters (voltage frequency and/or phase angle information) so that they can be executed under digital signal processing cards or any real-time hardware type. On the other hand, the short-term corrective action stage (S-TPAS) prioritizes the accuracy and fast dynamic response than the computation burden and the aiding parameters as this process can be performed offline to provide a detailed analysis of the voltage/current under different operating modes. Unfortunately, the ship classifications standards and rules that deal with power quality issues [9] did not distinguish between the (S-TPAS) stage and (L-TPAS) in proposing the appropriate harmonic assessment method that fits each action.

The most utilized method in data analysis and signal processing is the fast Fourier transform (FFT) due to its simplicity, and capability of performing harmonic spectral analysis for both offline and online applications. Therefore, most industrial power quality analyzers and data recorders depend on FFT to perform harmonics estimation. Besides, the dominant IEC standards 61000-4-7/30 and the under-revised IEEE 519 always recommend this method. Unfortunately, the FFT is a frequency-dependent technique, which implies that it can neither estimate the frequency nor perform appropriately under system frequency drifts. Hence, the application of the FFT on its form to A-ESs is not efficient due to the large frequency variation that results in the spectral leakage and picket-fence effect. For offline applications, the use of frequency estimation techniques such as phase/frequency locked-loop (PLL/FLL) cannot be efficient as the PLL/FLL can only be applied in online applications due to their closed-loop feedback system characteristics. Furthermore, designing the PLL/FLL controller requires complex system stability analysis that needs professionals to be performed. To avoid this predicament, this paper proposes two optimized open-loop algorithms, which overcome the weaknesses of the frequency dependency of the FFT to assess the energy quality of shipboard microgrids. The contributions of this paper are summarized below:

- Proposing an optimized signal periodicity independent algorithm, which is an offline-based energy quality analyzing technique for S-TPAS of shipboard microgrids. This technique incorporates the eigenvalue solution inside the short-time fast Fourier transform (ST-FFT), which can effectively estimate the system frequency in an open-loop pattern without relying on the signal periodicity to adapt the FFT sliding window size. Consequently, this algorithm can provide a comprehensive harmonics analysis with a fast transient response even under large system frequency drifts without causing spectral leakage or picket fence effect.
- Proposing an enhanced algorithm, which is an online-based energy quality assessing technique dedicated to L-TPAS. This algorithm is based on cascading three moving average filters (MAFs) with different short window sizes inside the discrete Fourier transform and true RMS blocks. Consequently, as it will be demonstrated in the analysis, this structure enhances the harmonics rejection capability of the algorithm to estimate the THD accurately even under the existence of non-characteristic harmonics and frequency drifts with a short transient response and efficient computation burden.
- Delivering a comparative study of the most popular methods for energy quality assessment in terms of resolution, accuracy, and dynamic response under adverse grid conditions.

Simulation and experimental results are carried out to demonstrate the efficacy of the proposed methods.

2. Short-term corrective action based harmonics distortion assessment

The S-TPAS needs a very accurate method not to only assess the THD of the distorted data, but to provide also accurate information about the type of the harmonics (e.g., odd harmonics, even harmonics, interharmonics, subharmonics, etc.) and their order. There are many techniques applied for harmonics estimation such as synchronous reference frame (SRF) [10], PQ-theory [11], cascaded delayed signal cancelation technique [12,13], real and complex coefficient filters [14,15],artificial neural networks [16,17], wavelet packet decomposition [18], least-squares technique [19,20], Kalman filter [21], discrete Fourier transform (DFT) [22,23]. However, these methods are generally applied to selectively estimate the dominant harmonics or only the fundamental component. Hence, their application is very suitable for active power filters, fixed panel instrumentation, and electronic trip units of circuit-breakers. Moreover, some of these techniques have a closed-loop system, which means that they are not suitable for offline applications. Furthermore, most of the techniques used in the literature are not applied in industrial applications as most of these industrial power quality analyzers and measurement instruments depend on the ST-FFT due to its simplicity and ability to estimate a large range of harmonics that goes up to the aliasing point [24,25].

The ST-FFT is, however, a frequency-dependent technique, which implies that its accuracy degrades under frequency drifts due to the spectral leakage phenomenon. This issue can be avoided by adapting the window size of the ST-FFT with the instantaneous frequency of each cycle. Unfortunately, the most used frequency estimation techniques such PLL/FLL are closed-loop systems that work only online [26]. Hence, their application to estimate the frequency offline to adapt the FFT under frequency drifts is not possible [27]. Zero cross techniques can work effectively offline. However, under harmonically contaminated data, their performance tends to worsen. In order to overcome this issue, ship classifications standards and rules that are set following the dominant IEC standards 61000-4-7/30 [28,29] and the under-revised IEEE 519 [30] recommend the extension of the window width of FFT to 10/12 cycles of the fundamental to attenuate the spectral leakage caused by the frequency drifts and the interharmonics. However, as the A-ESs are distinguished by the large dynamics, following the standard recommendation will not be practical due to the large transient response. Several windowed interpolated-based FFT techniques are proposed in the literature to reduce the effect of the spectral leakage such as Hanning window [31], Hamming window [32], Blackman-Harris window [32]. These techniques are applied to smoothly truncate the side lobes caused by the triangular window to enhance the data synchronization with the FFT width. However, these methods enlarge the width of the main lobe, which consequently affects the resolution. Furthermore, using these windows separate the fundamental component into one main component and two adjacent components, then the real value is estimated by subgrouping the three components. Hence, the existence of the interharmonics that are adjacent to the fundamental perturbs their accuracy. Other methods apply the fundamental identification and replacement technique [33]. However, the authors did not validate its performance in terms of the dynamic response.

The matrix pencil method (MPM) can be a very effective tool to estimate the frequencies of each harmonic in an offline pattern using the singular value decomposition (SVD) and eigenvalue solution, then adapt the least square solution for each cycle to estimate accurately the amplitudes of the harmonics under frequency drifts [34,35]. Hence, its application to A-ESs is very effective [36]. However, as will be demonstrated in the following analysis, the MPM resolution tends to worsen if the sampling time of the data increases. Consequently, the number of harmonics estimated by the ST-FFT will be much higher than the one estimated by the MPM. Therefore, the proposed method is a very effective approach compared to the MPM when the sampling frequency of the data is low. The proposed method applies the eigenvalue solution to estimate only the fundamental frequency, and then adapt the sliding window width of the FFT to estimate accurately the harmonics up to the aliasing point. The DFT may be expressed as:

$$X(k) = \sum_{n=0}^{N-1} x(n)\, W_N^{kn}\ k = 0, \ldots, N-1 \tag{1}$$

where $x(n)$ is input data, $W_N = e^{-j2\pi/N}$, k is the step time, N is the number of samples. The development of the FFT can be related to C. F. Gauss's work in 1805 when he wanted to incorporate the orbit of asteroids Pallas and Juno from sample observations. In 1965, Cooley-Tukey has optimized the structure of the FFT to be executed on a computer platform [24]. The FFT is a method that operates the DFT in an effective way to achieve the same results with a calculation burden that is decreased from $O(N^2)$ to $O(NlogN)$ [37]. The easier and common method of Cooley-Tukey is the radix-2 decimation-in-time and decimation-in-frequency. The main idea of this technique is to factorize the input sequence $x(n)$, which contains the number of samples N into two sizes of $N/2$ that are categorized as even-indexed size ($x_{2m} = x_0, x_2, \ldots, x_{N-2}$) and odd-indexed size ($x_{2m+1} = x_1, x_3, \ldots, x_{N-1}$) and expressed as:

$$X(k) = \sum_{m=0}^{N/2-1} x(2m) W_N^{k(2m)} + \sum_{m=0}^{N/2-1} x(2m+1) W_N^{k(2m+1)} \tag{2}$$

$$X(k) = \overbrace{\sum_{m=0}^{N/2-1} x(2m) W_N^{k(2m)}}^{even-indexed\ vectors\ of\ x(n)} + W_N^k \overbrace{\sum_{m=0}^{N/2-1} x(2m+1) W_N^{k(2m)}}^{odd-indexed\ vectors\ of\ x(n)} \tag{3}$$

where $W_N = e^{-j2\pi/N}$, and $k = 0, \ldots, N-1$. From (3), the formulation of $X(k+\frac{N}{2})$ can be easily achieved as:

$$X(k+\frac{N}{2}) = \sum_{m=0}^{N/2-1} x(2m) W_N^{(k+\frac{N}{2})m} + W_N^{(k+\frac{N}{2})} \sum_{m=0}^{N/2-1} x(2m+1) W_N^{(k+\frac{N}{2})m} \tag{4}$$

$$X(k+\frac{N}{2}) = \sum_{m=0}^{N/2-1} x(2m) W_N^{mk2} - W_N^k \sum_{m=0}^{N/2-1} x(2m+1) W_N^{mk2} \tag{5}$$

The equations of $X(k)$ and $X(k+\frac{N}{2})$ contain the $N/2$ size of radix-2, which lessen the DFT size from N to $N/2$. Note that (3) and (5) are similar except the second term of (3) is negative, which delineates a size-2 DFT that is sometimes known as butterfly operations. In case the number of radices is high, then the application of the size-N DFT is more feasible, where its decomposition into size-$N/2$ DFTs is known in some cases as Danielson–Lanczos lemma.

The spectral leakage effect occurs usually when the frequency of the input data $x(n)$ does not match the signal periodicity of the FFT. This issue is very common in A-ESs due to the pulsed loads that absorb a large amount of power in a short time. According to (1), The DFT window size in terms of frequency is expressed as:

$$f \hat{=} k/N \tag{6}$$

where f is the fundamental frequency of $x(n)$. The proposed method estimates f using the eigenvalue solution in an open-loop pattern to adapt the window size of the DFT/FFT as:

$$f = \frac{f_s}{2\pi} Im\left(log(\lambda_{1,2})\right) \tag{7}$$

where f_s is the sampling frequency, log is the logarithm function, Im denotes the imaginary part of the equation, and $\lambda_{1,2}$ are the eigenvalues that correspond to the fundamental frequency and calculated using the eigenvalue solution formulas as presented in (8), which can be simplified to (9):

$$[G_2] - \lambda[G_1] = 0 \tag{8}$$

$$[G_1]^+[G_2] - \lambda[I] = 0 \tag{9}$$

where λ are the eigenvalues of all frequencies in the signal, $[I]$ denotes the identity matrix, and $+$ refers to the Moore-Penrose pseudoinverse [35]. The matrices $[G_1]$ and $[G_2]$ are the inverse SVDs with different right singular vectors that are expressed as:

$$[G_1] = [U][\sum][V_a]^* \tag{10}$$

$$[G_2] = [U][\sum][V_b]^* \tag{11}$$

where * denotes the transpose of the matrix. In (10), $[U]$ and $[V_a]$ are the matrices that contain the left and right singular vectors of $[G_1]$ that contain respectively the orthonormal eigenvectors of $[G_1]\cdot [G_1]^*$ and $[G_1]^*\cdot [G_1]$. The definition of the matrices of (11) is similar to those of (10). The matrix $[\sum]$ contains the square roots of the non-negative eigenvalues or sometimes referred to as the singular values σ_i of the products $[G_1]\cdot [G_1]^*$ and $[G_1]^*\cdot [G_1]$ for (10), and $[G_2]\cdot[G_2]^*$ and $[G_2]^*\cdot [G_2]$ for (11). Each two of σ_i usually correspond to one frequency. The matrices $[V_a]$ and $[V_b]$ are calculated by removing the last and first rows of the matrix $[V]$, respectively as:

$$[V_a] = [V(1:N-L-1,\ 1:M)] \tag{12}$$

$$[V_b] = [V(2:N-L,\ 1:M)] \tag{13}$$

where L is referred to as the pencil parameter [38], and it is usually selected as $\frac{N}{3} \leqslant L \leqslant \frac{N}{2}$ to improve the noise immunity of the algorithm [39,40]. M is the tolerance, which is selected to the higher existent harmonic for noiseless signals. However, for noisy signals, according to the best authors' knowledge, there is no straightforward method to calculate it. Therefore, some papers use approximated calculations by selecting M to a certain singular value σ_A that ensures $\sigma_A/\sigma_{max} = 10^p$ [34,35], where P refers to the significant decimal digits of the distorted signal. In case the ratio of the singular values of this division exceeds p, they appear as essential noise. Hence, choosing M less than that value of the division results in canceling the noise.

The matrix $[V]$ contains the right singular vectors of the Hankel matrix $[x]$ that is obtained using the SVD as:

$$[x] = [U][\sum][V]^* \tag{14}$$

The Hankel matrix $[x]$ is built based on the input data $x(n)$ as:

$$[x] = \begin{bmatrix} n(1) & n(2) & \ldots & n(L+1) \\ n(2) & n(3) & \ldots & n(L+2) \\ \vdots & \vdots & \ddots & \vdots \\ n(N-L) & n(N-L+1) & \ldots & n(N) \end{bmatrix}_{(N-L)(L+1)} \tag{15}$$

The first advantage of the FFT compared to the MPM is the higher number of harmonics that can be estimated at certain sampling time T_s. Inside the matrix $[\sum]$ in (14), the singular values σ_i appear as pair numbers, where each pair represent one harmonic frequency. Furthermore, the size of the Hankel matrix in (15) is limited by the parameter L that is constrained between $\frac{N}{3} \leqslant L \leqslant \frac{N}{2}$. Hence, the maximum number of harmonics estimated by the MPM is equivalent to $(L+1)/2$. However, the proposed method estimates the frequency using (6)-(15) then adapts the window width of the FFT with a maximum number of harmonics $f_s/2$. Fig. 3 presents the maximum number of harmonics that is estimated by the MPM and the proposed method in terms of sampling frequency and window width (frequency). It is clear that the MPM maximum number of harmonics is half of that of the proposed method when $L = N/2$. Decreasing L towards $N/3$ to enhance the noise resilience results in decreasing the maximum number of harmonics estimated by the MPM.

Another major difference between the proposed method and the MPM is the spectral resolution. The resolution of the FFT is defined as:

$$S_{r\_FFT} = f_s/N \tag{16}$$

Though the MPM can estimate both harmonics and interharmonics, its maximum number of the exponentials that can be extracted is restrained in the interval $N/6 \leqslant f_{max} \leqslant N/4$. Thus, there is, unfortunately, no linear equation that can represent the MPM spectral resolution.

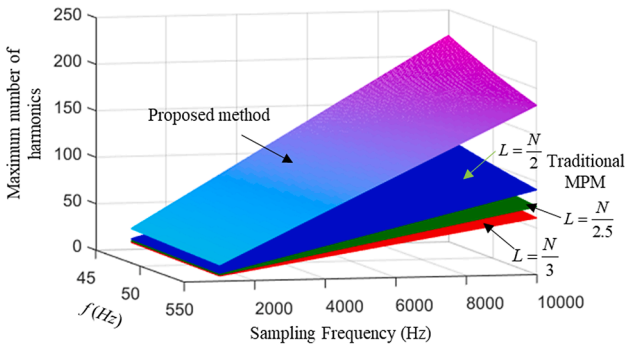

Fig. 3. Maximum number of harmonics estimated by the MPM and the proposed method.

However, an efficient way to visualize the resolution of the MPM is by calculating the average difference of the exponentials in terms of the sampling time T_s and algorithm window size as:

$$S_{rMPM} = 1/(T_s L) \tag{17}$$

Fig. 4 is presented to portrait the difference between the proposed method based on the ST-FFT and the MPM in terms of sampling time and algorithm window size (frequency). It is obvious that the variation of the sampling time does not influence the proposed method resolution. However, the MPM average resolution is proportional to the sampling time. Hence, for certain window sizes, there is a point where the proposed method and the MPM have the same resolution, increasing the sampling time to less than these points enables the proposed method to offer better resolution than the MPM and vice versa for decreasing it. Therefore, the proposed method's performance is superior when the entered data have a higher sampling time than the points shown in Fig. 4. Creating interpolating points in the Hankel matrix can enhance the MPM resolution [36]. However, this method cannot solve the resolution issue when the sampling time is high. Besides, the computation burden of this method is very high as the SVD will compute double size matrices and the accuracy of extracting high-order harmonics tends to worsen when the distortion of the signal is high.

3. Long-term preventive action based harmonics distortion assessment

Long-term preventive action techniques are usually employed online using some smart measurement instruments such as smart meters and power quality analyzers to measure the signal distortion and update the power management system to take action in case the distortion becomes severe. The FFT/DFT are the widely applied methods in these industrial measurement instruments due to their simplicity [41,42] and are often recommended by the power quality standards [9]. As mentioned in

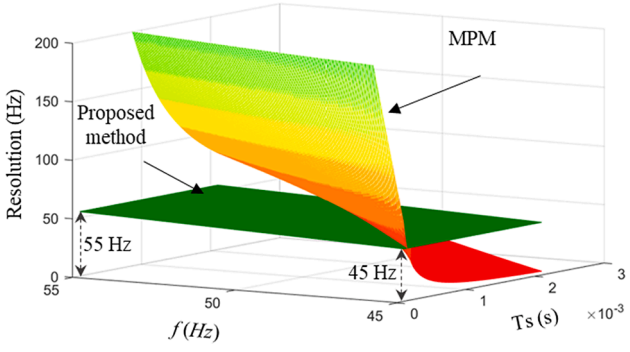

Fig. 4. Resolution of the MPM and the proposed method in terms of the sampling time and window size.

previous sections, the main deficiency of the DFT/FFT is the frequency dependency, which means that if the supply frequency varies, the accuracy of the DFT/FFT tends to worsen. In order to avoid this issue, the most often used power quality classification standards such as IEC standards 61000-4-7/30 [28,29] and the under-revised IEEE 519 standards [30] recommend the extension of the window size of the DFT to 10/12 cycles of the fundamental one. Unfortunately, this method has a very slow dynamic response, which makes its application to A-ESs not effective due to the large transients.

There are several ways of calculating the THD or the signal distortion [43,44]. One of the effective and fast methods is presented in Fig. 5. This method starts by computing the fundamental component of the signal using the ST-DFT. In the domain $n \in [0, N-1]$, the ST-DFT expression is:

$$x(n) = \frac{1}{N}\sum_{k=0}^{N-1} X(k)\, e^{j2\pi kn/N},\ n \in \mathbb{Z} \tag{18}$$

where $X(K)$ is the input data, $e^{j2\pi kn/N} = cos(\frac{2\pi}{N}kn) + j{\cdot}sin(\frac{2\pi}{N}kn)$, substituting this expression in (18) results in:

$$x(n) = \frac{1}{N}\sum_{k=0}^{N-1}\left(X(k)\left(cos(\frac{2\pi}{N}kn) + j{\cdot}sin(\frac{2\pi}{N}kn)\right)\right),\ n \in \mathbb{Z} \tag{19}$$

The term $\frac{1}{N}\sum_{k=0}^{N-1}X(k)$ inside (19) represents the same equation as the MAF [20]. The role of the MAF inside the DFT is to estimate the DC component that represents the aimed frequency, which is the fundamental component in this case. According to the Bode plot of the MAF depicted in Fig. 6, the ideal selection of the window size T_W of the MAF is 1 cycle to enable it to create notches at the harmonics of the order 6 h ± 1, harmonics caused by the unbalance (3rd harmonic and its multiple), even harmonics (2nd, 4th,6th, etc.), and the DC offset. Hence, these notches result in canceling all these harmonics and extracting only the fundamental component. However, under frequency variations, the tuning of these notches deviates from the aimed harmonics, which results in decreasing the accuracy of the MAF. The application of the PLL/FLL can adapt the MAF under frequency drifts. However, the PLL/FLL is a closed-loop feedback system, which requires careful stability analysis to avoid the instability and often distinguished my larger dynamic response (more than 2 cycles) [20]. Furthermore, the existence of the interharmonics, between every two harmonics tends the MAF performance to worsen. Using the IEC standards 61000-4-7/30 DFT (standard DFT) [28,29], which recommend a window size of 12 cycles results in creating several notches between every two harmonics as presented in Fig. 6. Hence, it can reject a large number of inerharmonics. However, this solution suffers from a long dynamic response, which implies that its application to A-ESs is not practical due to the large pulsed load variations in a short time. Generally speaking, in electrical power systems the interharmonics and even harmonics usually appear with low values compared to other harmonics due to the nonlinear load characteristics [1]. Hence, it will be demonstrated in this paper that the performance of the MAF can be improved when cascading three MAFs in series with different window sizes ($T_W = 0.02/2\ s$, $T_W = 0.02/4\ s$, $T_W = 0.02/2\ s$) as presented in Fig. 5 as:

$$x(n) = \frac{1}{N_2}\sum_{k=0}^{(N_2-1)}\left(\frac{1}{N_4}\sum_{k=0}^{(N_4-1)}\left(\frac{1}{N_2}\sum_{k=0}^{(N_2-1)} X(k)cos(\frac{2\pi}{N}kn)\right)\right) \tag{20}$$

$$y(n) = \frac{1}{N_2}\sum_{k=0}^{(N_2-1)}\left(\frac{1}{N_4}\sum_{k=0}^{(N_4-1)}\left(\frac{1}{N_2}\sum_{k=0}^{(N_2-1)} X(k)sin(\frac{2\pi}{N}kn)\right)\right) \tag{21}$$

where $N_2 = N/2$ and $N_4 = N/4$. Consequently, the MAF creates deep notches at several harmonics orders (odd harmonics, and the harmonics of the order 6 h ± 1) and their adjacent interharmonics as shown in the Bode plot of Fig. 6 that lead to reject these harmonics and diminish the adjacent interharmonics with the dynamic response of only one cycle.

Hence, the filtering performance will be improved by maintaining

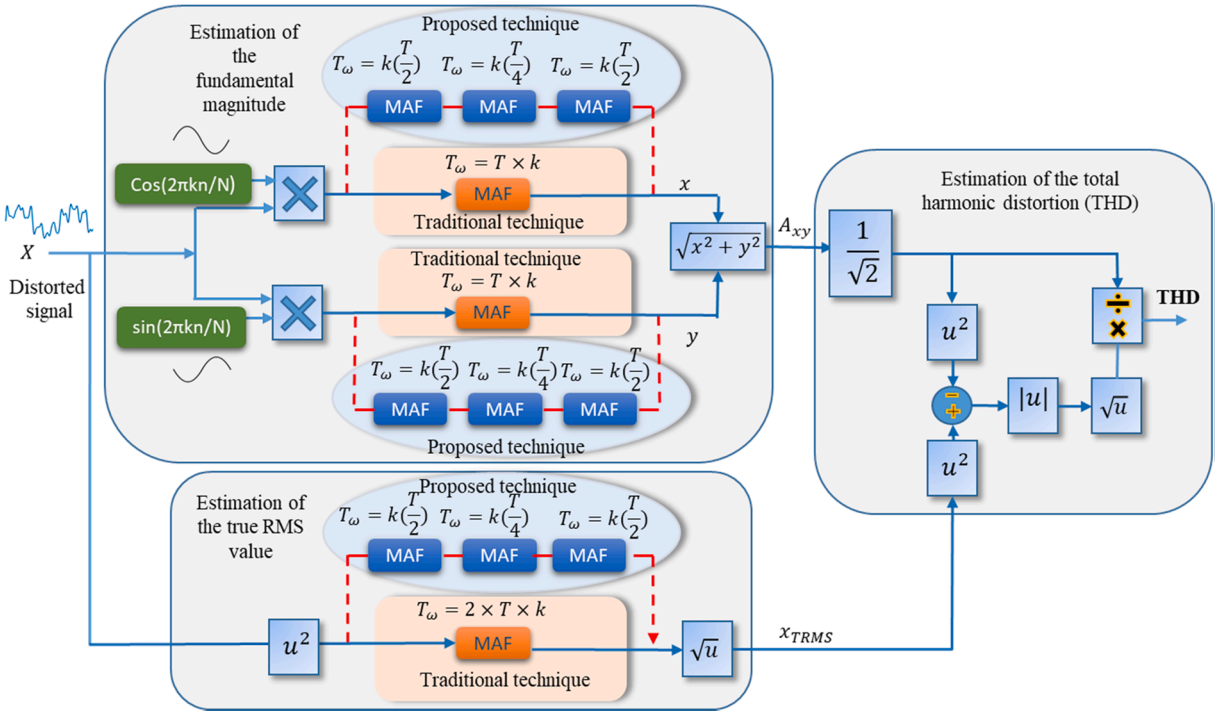

Fig. 5. Estimation of the THD using the proposed method.

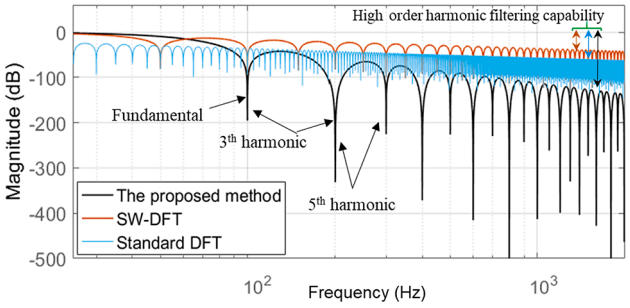

Fig. 6. Bode plot of the MAF with the proposed window size, window size recommended by the IEC standards, and window size of 1 cycle.

the same dynamic response of $T_W = 0.02$ *s*. It is noteworthy that when multiplying the distorted signal in cosines and sines (see (19)), the fundamental frequency order shifts to $h + 1$, and other harmonics orders get separated between the order $h + 1$ and h-1 as presented in Fig. 6. The key factor behind this characteristic is the structure of cascading three MAFs at the even harmonics, which results in enlarging their notches sizes and depths. Fig. 7 is added to further simplify the principle of the proposed method. It is clear that when setting the MAF window size to a half cycle (TW = 0.02/1s), it results in creating notches at the even harmonics. Cascading another MAF with TW = 0.02/4s further enhances the size and the depth of these notches at the dominant even harmonics frequencies (200 Hz, 400 HZ, 600 Hz …etc.) and enhances the attenuation of the bode magnitude at all harmonics with the increase of frequency order. Finally, adding the last MAF with half-cycle window size (TW = 0.02/1s) results in enlarging the notches of all these even harmonics and their depth. The advantage of enlarging the size of these notches is to create higher harmonics rejection capability at the adjacent interharmonics. Consequently, if an interharmonic appears or the system frequency variation occurs, the proposed method's efficacy remains high.

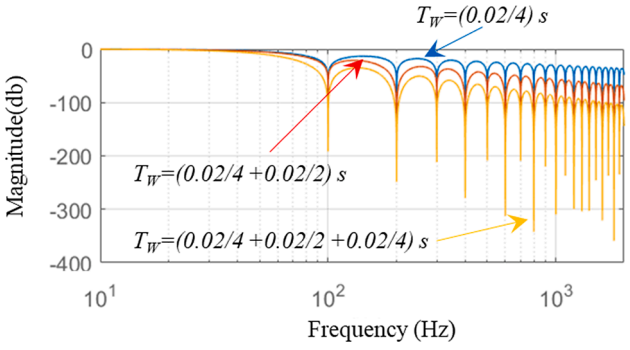

Fig. 7. Bode plot of the transfer function of the MAF with three cascaded blocks.

In addition, the application of the low-pass filter is not efficient due to low performance at lower-order harmonics. Fig. 8 presents the bode plot of a low-pass filter and the proposed MAF with the same total window size. It is clear that the magnitude of the low-pass filter is not low enough at lower order harmonics, which decreases its harmonics rejection capability. However, the proposed method acts as an ideal low-pass filter with very sharp notches at the aimed even harmonics, which can completely filter them. Seeking to decrease the magnitude of the low-pass filter at lower order harmonics results in increasing the transient response, which affects the efficacy of estimating the THD. Next,

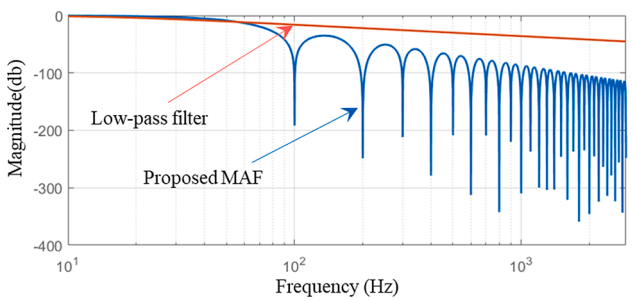

Fig. 8. Bode plot of a low-pass filter and the proposed MAFs.

the magnitude of the fundamental frequency is simply estimated as:

$$A_{xy} = \sqrt{x(n)^2 + y(n)^2} \tag{22}$$

The next step is to calculate the true RMS of the contaminated data as presented in (23). Similar to the previous procedure in (20)/(21), by cascading 3 of the MAF block inside the true RMS block (see (23) and Fig. 5) with window sizes set to $T_W = 0.02/2s$, $T_W = 0.02/4s$, and $T_W = 0.02/2s$, the harmonics rejection capability of this technique will be effectively improved.

$$x_{TRMS}(n) = \sqrt{\frac{1}{N_2}\sum_{k=0}^{(N_2-1)}\left(\frac{1}{N_4}\sum_{k=0}^{(N_4-1)}\left(\frac{1}{N_2}\sum_{k=0}^{(N_2-1)}(X^2(k))\right)\right)} \tag{23}$$

It is noteworthy that the terms $\frac{1}{N_2}\sum_{k=0}^{(N_2-1)}(X^2(k))$, $\frac{1}{N_4}\sum_{k=0}^{(N_4-1)}(A)$, and $\frac{1}{N_2}\sum_{k=0}^{(N_2-1)}(B)$ (where $A = \frac{1}{N_2}\sum_{k=0}^{(N_2-1)}(X^2(k))$, and $B = \frac{1}{N_4}\sum_{k=0}^{(N_4-1)}(A)$) that represent a series combination of the MAFs equations are a particular calculation inside the true RMS equation in (23), which computes the mean value of each window size (N_2, N_4, and N_2). After the calculation of the true RMS and the fundamental component of the input data, the THD will be computed as:

$$THD = \frac{\sqrt{\left|(x_{TRMS})^2 - \left(A_{xy}/\sqrt{2}\right)^2\right|}}{A_{xy}/\sqrt{2}}100\,\% \tag{24}$$

It is noteworthy for L-TPAS, the proposed method is sufficient to estimate the THD. However, for other applications that require information about each existing harmonic online, a similar model that is presented in Fig. 5 tuned at each aimed harmonic is necessary, which can increase the computation burden if the number of the aimed harmonics is high.

4. Numerical results and discussions

4.1. Numerical results of the short-term corrective action stage based harmonics distortion assessment

The numerical results are carried out under MATLAB/ Programming software. Fig. 9 depicts the performance of the proposed ST-FFT adapted with the eigenvalue solution method. The traditional ST-FFT and standard FFT are selected to be compared with the proposed method due to their large applications in industrial signal processing instruments and power quality analyzers. Besides, the MPM is selected as well to be compared with due to its efficient signal periodicity independent characteristic and popularity [34,36,38]. The first subplot of Fig. 9 presents the input data, which is harmonically contaminated with a THD of around 40% and a sampling time of 0.2 ms. The second subplot demonstrates the effectiveness of the proposed method in estimating the fundamental frequency of the input data in an open-loop pattern (without feedback closed-loop system). Hence, this method does not require any stability analysis or controller design. The last subplot presents the THD of the contaminated data estimated by the aforementioned methods. It is clear that the traditional MPM accuracy is acceptable before and after frequency variation. However, as the number of harmonics is high and the sampling frequency is a bit low (5 kHz), it results in a very high overshoot during the transients, and its accuracy under amplitude variation tends to worsen. This is clear in the harmonic spectrum of Fig. 10 (a), where there are many intruder frequency bins due to the poor resolution that causes erroneous information. The ST-FFT can accurately estimate the THD of the data under nominal frequency. However, when the frequency of the data drifts by 2%, its performance decreases resulting in some fluctuations. This can be visualized in the harmonic spectrum of Fig. 10 (b), which demonstrates the existence of the spectral leakage caused by the frequency variation. Though the standard FFT can provide good accuracy under frequency drifts, its transient response is very slow, which leads to erroneous information. This deficiency is obvious in Fig. 10 (c) where the spectral leakage and picket-fence effect appears to disturb the estimation accuracy. On the other hand, based on the eigenvalue solution, the accurate frequency of the proposed method that is estimated in an open-loop pattern (see Fig. 9, subplot. 2) enables the adoption of the ST-FFT under frequency drifts. Hence, the estimated THD of the proposed method follows the reference signal accurately. This evidence is clear in Fig. 10 (d), where the harmonic spectrum has neither the spectral effect nor the picket-fence effect under frequency drifts and offers a very fast transient response under magnitude variation.

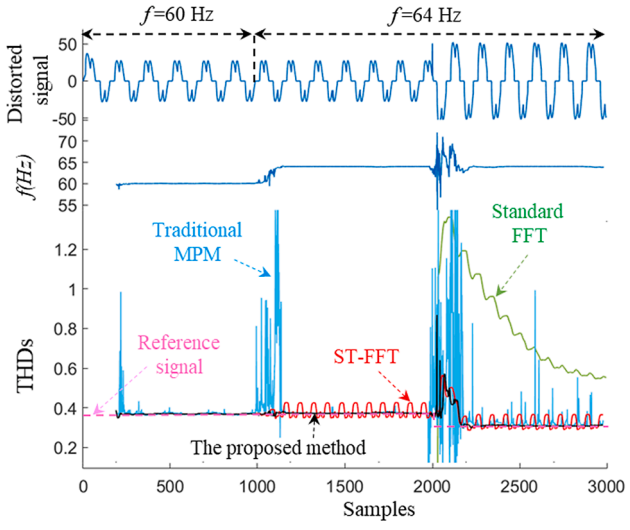

Fig. 9. Simulation results. Performance of the traditional MPM, ST-FFT, standard FFT, and the proposed method in estimating the harmonics distortion.

4.2. Numerical results of the long-term preventive action based harmonics distortion assessment method

The numerical results are carried out under MATLAB/Simulink software. Fig. 11 presents the performance of the proposed ST-DFT, which is based on cascading 3 MAFs with different window sizes as explained in section III. The first subplot portrays the input data, which is distorted with harmonics and interharmonics. The remaining subplots present the true RMS, fundamental component, and the THD, respectively. It is clear that the traditional ST-DFT accuracy is not satisfactory due to the fluctuations caused by the interharmonics. Besides, the variation of the frequency at the instance 0.3 s tends the performance of the traditional ST-DFT to worsen. The standard DFT can overcome the weakness of the interharmonics. However, its dynamic response is very long, which results in erroneous information, particularly when estimating the fundamental components, in which the results demonstrated that the estimated signal does not follow the reference one, which results in a wrong THD estimation. On the other hand, the proposed method provides satisfactory accuracy even under magnitude and frequency variations, which validates the analysis performed in the section. III.

5. Experimental results and discussions

5.1. Experimental results of the short-term corrective action stage based harmonics distortion assessment

The experimental analysis to verify the performance of the proposed FFT adapted by the eigenvalue solution is attained by analyzing the data of a bulk carrier ship presented in Fig. 12 (a). The operation mode in which the data was recorded is during the use of the windlass, and the mooring winches that are depicted in Fig. 12 (b). The measurement

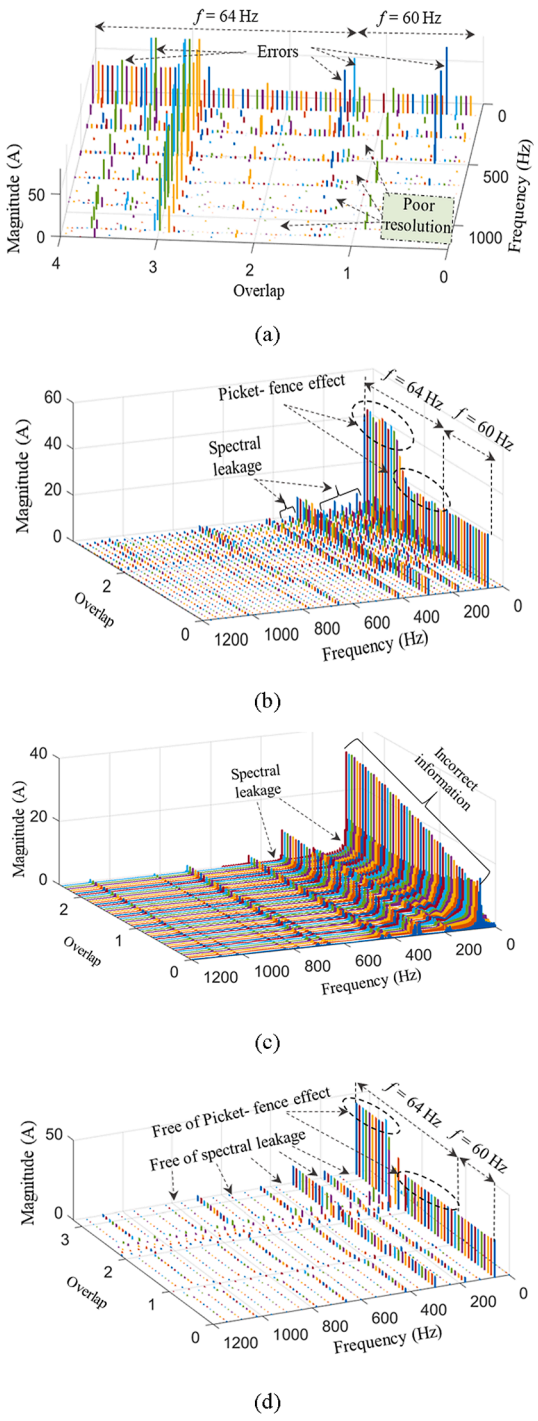

Fig. 10. Simulation results. Harmonic spectrums of the input data extracted by: (a) the traditional MPM, (b) ST-FFT, (c) standard FFT, and (d) the proposed method.

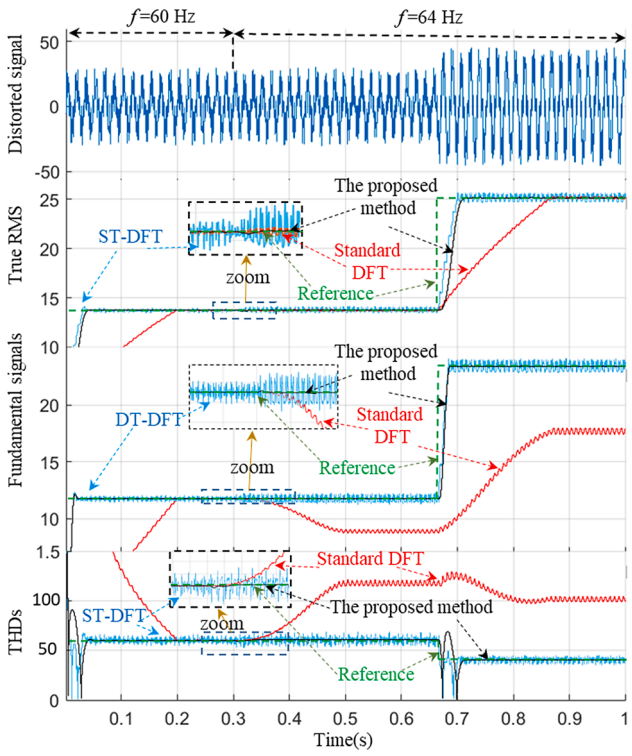

Fig. 11. Simulation results. Performance of the proposed ST-DFT based on three cascaded MAFs, traditional ST-DFT, and standard DFT in estimating the THD.

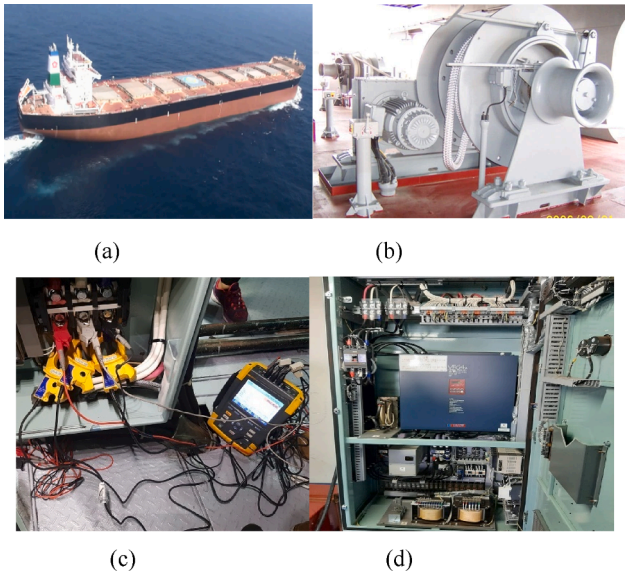

Fig. 12. Experimental analysis. (a) Picture of the chosen bulk carrier ship. (b) Windlass and mooring winch. (c) Measurement device (Fluke). (d) Main switchboard of the Windlass and mooring winches.

device type Fluke presented in Fig. 12 (c) is selected to record the data from the main switchboard shown in Fig. 12 (d).

Fig. 13 presents the performance of the proposed method in analyzing the current THD of a bulk carrier ship, and the results are compared with traditional ST-FFT and standard FFT. The first subplot presents the experimental data, which is affected by the harmonics. The second subplot presents the measured THD of the input data, and the last subplot presents the system frequency that is estimated by the proposed method in an open-loop pattern. Due to the large dynamic response of the loads, and low switching frequency of the analyzed data (5 kHz), the traditional MPM fails to extract the THD resulting in a large disturbance. This disturbance is clear in the harmonics spectrum of Fig. 14 (a), which contains many intruder frequency bins due to the poor resolution that leads to erroneous information. It is noteworthy that the estimated frequency of the system has many variations due to the large dynamics. Hence, the traditional ST-FFT cannot be a good choice due to the large oscillations. These oscillations have resulted from the spectral leakage depicted in the harmonic spectrum of Fig. 14 (b). The standard FFT

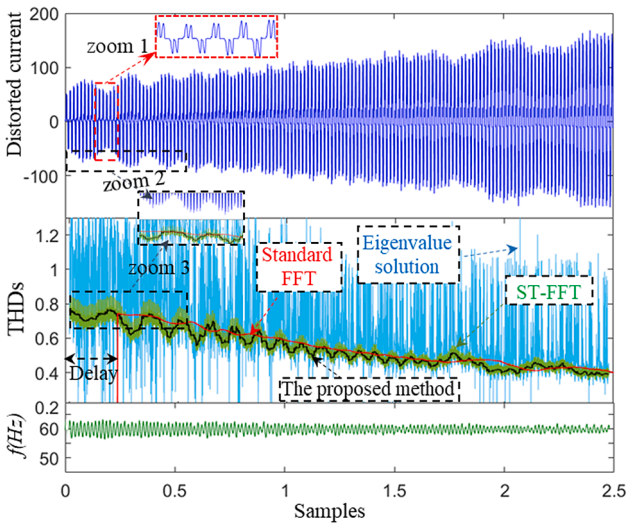

Fig. 13. Experimental results. Performance of the traditional MPM, ST-FFT, standard FFT, and the proposed method in estimating the harmonics distortion.

overcomes the oscillations caused by the traditional ST-FFT. However, due to its large window size, it makes a large delay and cannot follow the fast transients of the signal, which relatively causes erroneous information in short-term variations. This weakness will consequently result in the spectral leakage and picket-fence effect as presented in the harmonic spectrum of Fig. 14 (c). On the other hand, based on the frequency estimated by the eigenvalue solution, the proposed adapted ST-FFT does not struggle from any oscillations or overshoots and can follow the magnitude variations of the input data accurately with a fast response. This accuracy is demonstrated in Fig. 14 (d), where the harmonic spectrum is free of spectral leakage and picket-fence effect. Furthermore, the resolution of the spectrum of the proposed method is much better than that of the MPM, which validates the analysis provided in Section II.

5.2. Experimental results of the long-term preventive action based harmonics distortion assessment

Fig. 15 presents the experimental setup, which is developed to validate the efficacy of the proposed ST-DFT based on cascaded MAFs to work in real-time applications under a digital signal processor (dSPACE-1006). The right side of Fig. 15 is a programmable source (Chroma, model 61845), which can generate the desired signal. The sampling frequency is set to *100 kHz*.

Fig. 16 presents the performance of the proposed ST-DFT based on the cascaded MAFs, which is compared with traditional ST-DFT, and standard DFT. It is evident that the ST-FFT fails to provide an accurate assessment of the fundamental frequency and the true RMS due to the existence of the interharmonics. Though this technique provides a fast transient response under frequency variation (it takes one cycle to reach the steady state), its performance tends to worsen when the frequency changes from 60 Hz to 64 Hz in the instant 0.18 s. The standard DFT can overcome the weakness of the ST-FFT under the existence of interharmonics. However, when the frequency drifts from 60 Hz to 64 Hz it results in erroneous information of the fundamental component due to the very long transient response (12 cycles), and thus tends the accuracy of the estimated THDs to worsen. On the other hand, the proposed method can provide very accurate estimation even under the existence of interharmonics and frequency variation with a very fast transient response (0.025 s), which validates the simulation results.

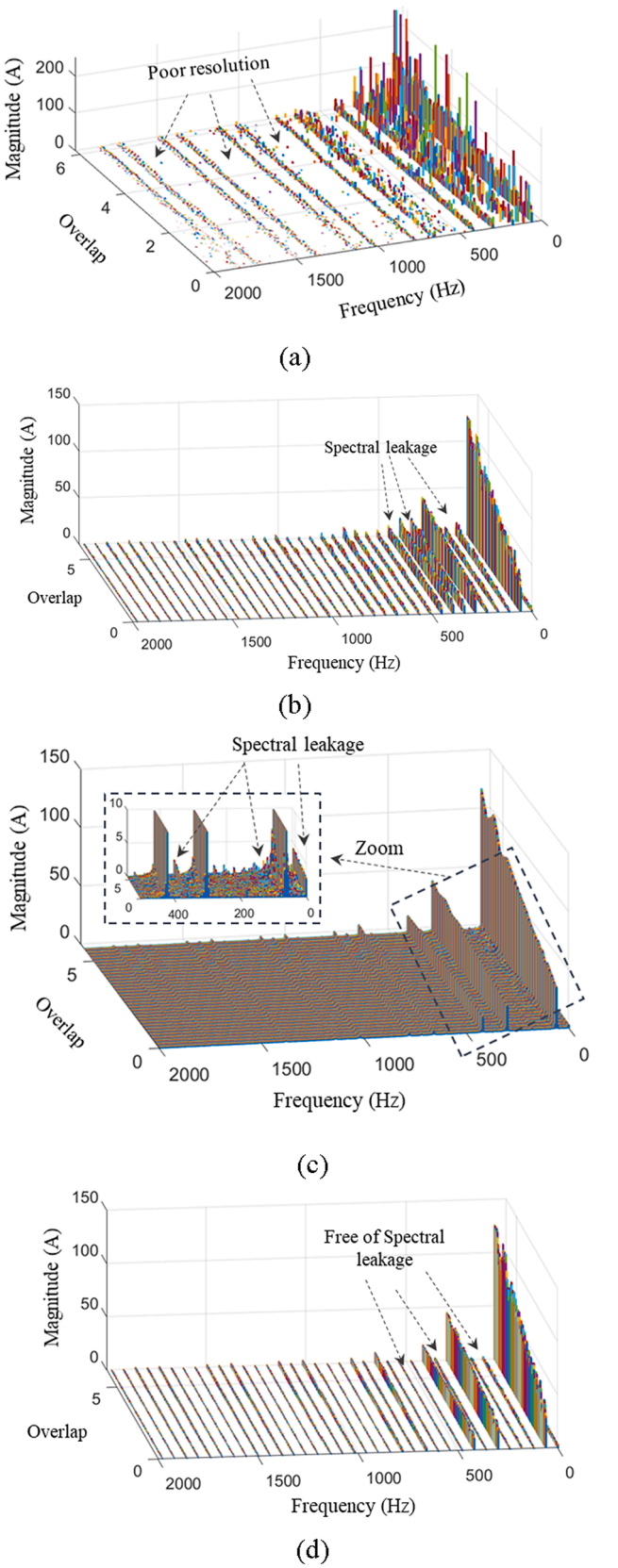

Fig. 14. Experimental results. Harmonic spectrums of the input data extracted by: (a) the traditional MPM, (b) ST-FFT, (c) standard FFT, and (d) the proposed method.

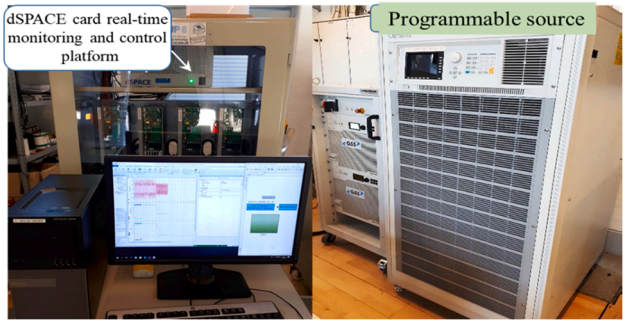

Fig. 15. Experimental setup for control and validation of the proposed method.

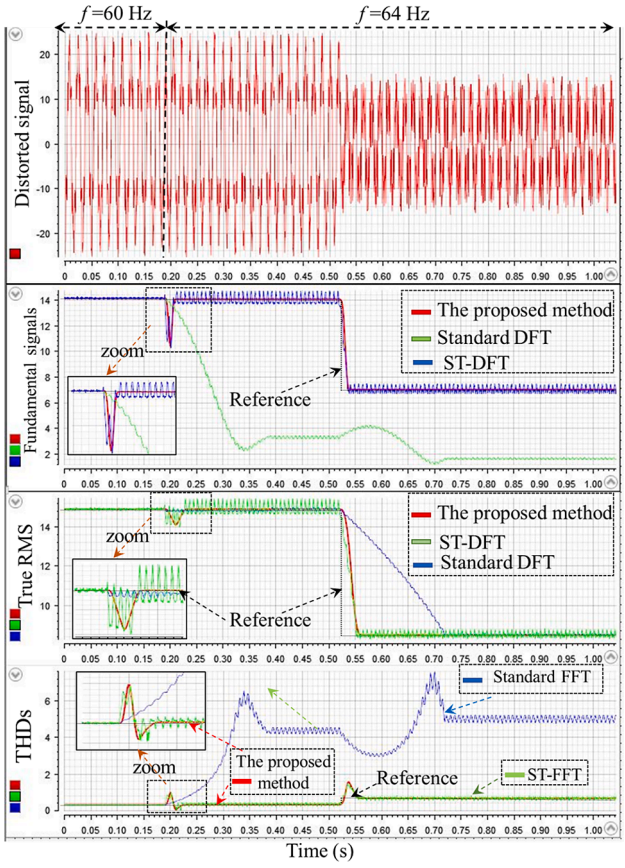

Fig. 16. Experimental results. Performance of the proposed ST-DFT based on three cascaded MAFs, traditional ST-DFT, and standard DFT in estimating the THD.

6. Conclusion

This paper proposed two effective open-loop algorithms to assess the harmonics distortion for S-TPAS and L-TPAS of A-ESs. The first algorithm is dedicated to S-TPAS and its contribution is based on adapting the ST-FFT window size using the eigenvalue solution to become more accurate with a very fast dynamic response under large frequency drifts. It was demonstrated in the simulation and experimental results that the eigenvalue solution can estimate the frequency of the input data accurately in an open-loop manner. Hence, the proposed method does not require any complicated stability analysis or controller design. Moreover, it was demonstrated in the analysis and results that this proposed method can provide better resolution than the traditional MPM when the sampling frequency is low. Besides, in contradiction to traditional ST-FFT and standard FFT that struggle from spectral leakage and picket-fence effect, the harmonic spectrum of the proposed method is free from these effects even when the frequency drifts.

The second algorithm is dedicated for L-TPAS and it is based on cascading three MAFs with different short window size tuned at $T_W = 0.02/4\ s$, $T_W = 0.02/2\ s$, $T_W = 0.02/4\ s$ inside the DFT and true RMS blocks. Consequently, based on the simulation and experimental results, it was proved that the cascaded MAFs create very deep notches at the characteristic and non-characteristic harmonics. Consequently, this feature leads to enhances the harmonics rejection capability of the algorithm and provides a fast dynamic response under the existence of interharmonics and large frequency drifts without adding any synchronization techniques (PLL/FLL).

CRediT authorship contribution statement

Yacine Terriche: Conceptualization, Methodology, Software, Validation. **Abderezak Lashab:** Conceptualization, Formal analysis, Software, Validation. **Halil Çimen:** Validation, Investigation. **Josep M. Guerrero:** Supervision, Project administration. **Chun-Lien:** Writing - review & editing, Visualization. **Juan C. Vasquez:** Supervision, Project administration.

Declaration of Competing Interest

The authors declare that they have no known competing financial interests or personal relationships that could have appeared to influence the work reported in this paper.

References

[1] Control of Harmonics in Electrical Power Systems, American Bureau of Shipping Guidance; 2006.
[2] Lai K, Illindala MS. A distributed energy management strategy for resilient shipboard power system. Appl Energy 2018;228:821–32.
[3] Chai M, Bonthapalle DR, Sobrayen L, Panda SK, Wu D, Chen XQ. Alternating current and direct current-based electrical systems for marine vessels with electric propulsion drives. Appl Energy 2018;231:747–56.
[4] Rules for Building and Classing Steel Vessels, American Bureau of Shipping, Houston, TX, USA; 2008.
[5] Terriche Y et al. Power quality and Voltage Stability improvement of Shipboard Power Systems with Non-Linear Loads. In: *2019 IEEE International Conference on Environment and Electrical Engineering and 2019 IEEE Industrial and Commercial Power Systems Europe (EEEIC / I&CPS Europe)*; 2019. p. 1–6.
[6] Li J, Yang Q, Mu H, Le Blond S, He H. A new fault detection and fault location method for multi-terminal high voltage direct current of offshore wind farm. Appl Energy 2018;220:13–20.
[7] Moussa MA, Boucherma M, Khezzar A. A Detection Method for Induction Motor Bar Fault Using Sidelobes Leakage Phenomenon of the Sliding Discrete Fourier Transform. IEEE Trans Power Electron Jul. 2017;32(7):5560–72.
[8] Mary RMSQ. RMS Queen Mary 2 Report No 28/2011. no. 28; 2011.
[9] Mindykowski J. Case Study—Based Overview of Some Contemporary Challenges to Power Quality in Ship Systems. Inventions 2016;1(4):12.
[10] Campos-Gaona D, Pena-Alzola R, Monroy-Morales JL, Ordonez M, Anaya-Lara O, Leithead WE. Fast selective harmonic mitigation in multifunctional inverters using internal model controllers and synchronous reference frames. IEEE Trans Ind Electron Aug. 2017;64(8):6338–49.
[11] Rachid A, Fadil HE, Koundi M, Idrissi ZE, Tahri A, Giri F, et al. PQ Theory-Based Control of Single-Stage V2G Three-Phase BEV Charger for High-Voltage Battery. IFAC-PapersOnLine 2019;52(29):73–8.
[12] Golestan S, Ramezani M, Guerrero JM, Monfared M. dq-Frame Cascaded Delayed Signal Cancellation- Based PLL: Analysis, Design, and Comparison With Moving Average Filter-Based PLL. IEEE Trans Power Electron Mar. 2015;30(3):1618–32.
[13] Terriche Y, et al. Adaptive CDSC-Based Open-Loop Synchronization Technique for Dynamic Response Enhancement of Active Power Filters. IEEE Access 2019;7:96743–52.
[14] Guo X, Wu W, Chen Z. Multiple-Complex Coefficient-Filter-Based Phase-Locked Loop and Synchronization Technique for Three-Phase Grid-Interfaced Converters in Distributed Utility Networks. IEEE Trans Ind Electron Apr. 2011;58(4):1194–204.
[15] Terriche Y, Golestan S, Guerrero JM, Vasquez JC. Multiple-Complex Coefficient-Filter-Based PLL for Improving the Performance of Shunt Active Power Filter under Adverse Grid Conditions. In: IEEE Power and Energy Society General Meeting; 2018, vol. 2018-August.
[16] Wang C, Zhang H, Ma P. Wind power forecasting based on singular spectrum analysis and a new hybrid Laguerre neural network. Appl Energy Feb. 2020;259:114139.

[17] Lai LL, Chan WL, Tse CT, So ATP. Real-time frequency and harmonic evaluation using artificial neural networks. IEEE Trans Power Deliv 1999;14(1):52–9.
[18] Eren L, Unal M, Devaney MJ. Harmonic Analysis Via Wavelet Packet Decomposition Using Special Elliptic Half-Band Filters. IEEE Trans Instrum Meas Dec. 2007;56(6):2289–93.
[19] El Zawawi A, Youssef KH, Sebakhy OA. Recursive least squares Harmonic identification in active power filters. European Control Conference (ECC) 2007; 2007:4645–50.
[20] Terriche Y, Guerrero JM, Vasquez JC. Performance improvement of shunt active power filter based on non-linear least-square approach. Electr Power Syst Res 2018;160:44–55.
[21] Nie X. Detection of Grid Voltage Fundamental and Harmonic Components Using Kalman Filter Based on Dynamic Tracking Model. IEEE Trans Ind Electron 2019:1.
[22] Chiu YJ, Leon Yu T. A discrete Fourier transform-based fuel concentration and permeation sensing scheme for low temperature fuel cells. Appl. Energy 2014;121: 123–31.
[23] Nicolae PM, Popa DL. Real-time implementation of some fourier transform based techniques for fundamental harmonic detection using dSPACE. In: *2016 18th European Conference on Power Electronics and Applications, EPE 2016 ECCE Europe*; 2016.
[24] Khafidli MK, Prasetyono E, Anggriawan DO, Tjahjono A, Syafii MHRA. Implementation AC Series Arc Fault Recognition using Mikrokontroller Based on Fast Fourier Transform. In: *2018 International Electronics Symposium on Engineering Technology and Applications, IES-ETA 2018 – Proceedings*; 2019. pp. 31–36.
[25] Subtirelu GE, Dobriceanu M, Linca M. Power quality analyser. In: *2017 10th International Symposium on Advanced Topics in Electrical Engineering, ATEE 2017*; 2017. p. 909–914.
[26] Ashabani M, Gooi HB, Guerrero JM. Designing high-order power-source synchronous current converters for islanded and grid-connected microgrids. Appl Energy 2018;219:370–84.
[27] Golestan S, Monfared M, Freijedo FD. Design-oriented study of advanced synchronous reference frame phase-locked loops. IEEE Trans Power Electron 2013; 28(2):765–78.
[28] IEC 61000-4-30 Edition 2.0- 2008-10- Electromagnetic compatibility (EMC) Part 4-30: Testing and measurement techniques- power quality measurements methods.
[29] IEC 61000-4-7 Edition 2 _ 2002-08. EMC _ Part 4-7: Testing and measurements techniques _ General guide on harmonics and interharmonics measurements and instrumentation, for power supply systems and equipment connected thereto.
[30] *519-2014 IEEE Recommended Practice and Requirements for Harmonic Control in Electric Power Systems.*
[31] Chintakindi SR, Varaprasad OVSR, Sarma DVSSS. Improved Hanning window based interpolated FFT for power harmonic analysis. In: *IEEE Region 10 Annual International Conference, Proceedings/TENCON*; 2016, vol. 2016-January.
[32] Sulistyaningsih, Putranto P, Daud P, Desvasari W. Fast Fourier Transform (FFT) Data Sampling using Hamming and Blackman Method for Radar. In: *Proceedings of 2018 International Conference on Electrical Engineering and Computer Science, ICECOS 2018*; 2019. p. 183–188.
[33] Wu M, Chen D, Chen G. New spectral leakage-removing method for spectral testing of approximate sinusoidal signals. IEEE Trans Instrum Meas 2012;61(5):1296–306.
[34] Sheshyekani K, Fallahi G, Hamzeh M, Kheradmandi M. A General Noise-Resilient Technique Based on the Matrix Pencil Method for the Assessment of Harmonics and Interharmonics in Power Systems. IEEE Trans Power Deliv Oct. 2017;32(5): 2179–88.
[35] Sarkar TK, Pereira O. Using the matrix pencil method to estimate the parameters of a sum of complex exponentials. IEEE Antennas Propag Mag 1995;37(1):48–55.
[36] Terriche Y, et al. A Resolution-Enhanced Sliding Matrix Pencil Method for Evaluation of Harmonics Distortion in Shipboard Microgrids. IEEE Trans Transp Electrif Sep. 2020;6(3):1290–300.
[37] Seo SM. A Fast IE-FFT Algorithm to Analyze Electrically Large Planar Microstrip Antenna Arrays. IEEE Antennas Wirel Propag Lett 2018;17(6):983–7.
[38] Hua Y, Sarkar TK. Generalized pencil-of-function method for extracting poles of an EM system from its transient response. IEEE Trans Antennas Propag 1989;37(2): 229–34.
[39] Hua Y, Sarkar TK. On the total least squares linear prediction method for frequency estimation. IEEE Trans Acoust Dec. 1990;38(12):2186–9.
[40] Terriche Y, Golestan S, Guerrero JM, Kerdoune D, Vasquez JC. Matrix pencil method-based reference current generation for shunt active power filters. IET Power Electron 2018;11(4):772–80.
[41] Zhou W, Ardakanian O, Zhang HT, Yuan Y. Bayesian Learning-Based Harmonic State Estimation in Distribution Systems with Smart Meter and DPMU Data. IEEE Trans Smart Grid 2020;11(1):832–45.
[42] Subhash B, Rajagopal V. Overview of smart metering system in Smart Grid scenario. In: *2014 Power and Energy Systems Conference: Towards Sustainable Energy, PESTSE 2014*; 2014.
[43] Mindykowski J. Power quality on ships: Today and tomorrow's challenges. *EPE 2014 - Proc. 2014 Int. Conf. Expo. Electr. Power Eng.*, no. Epe; 2014. p. 1–18.
[44] Mazzeo D, Oliveti G, Arcuri N. Influence of internal and external boundary conditions on the decrement factor and time lag heat flux of building walls in steady periodic regime. Appl Energy 2016;164:509–31.